

Integration of generalized B-spline functions on Catmull–Clark surfaces at singularities[☆]



Anna Wawrzinek^{*}, Konrad Polthier

Freie University Berlin, Germany

ARTICLE INFO

Keywords:

Subdivision surfaces
Catmull–Clark subdivision
Subdivision finite element
PDEs on surfaces
Isogeometric analysis

ABSTRACT

Subdivision surfaces are a common tool in geometric modelling, especially in computer graphics and computer animation. Nowadays, this concept has become established in engineering too. The focus here is on quadrilateral control grids and generalized B-spline surfaces of Catmull–Clark subdivision type. In the classical theory, a subdivision surface is defined as the limit of the repetitive application of subdivision rules to the control grid. Based on Stam's idea, the labour-intensive process can be avoided by using a natural parameterization of the limit surface. However, the simplification is not free of defects. At singularities, the smoothness of the classically defined limit surface has been lost. This paper describes how to rescue the parameterization by using a subdivision basis function that is consistent with the classical definition, but is expensive to compute. Based on this, we introduce a characteristic subdivision finite element and use it to discretize integrals on subdivision surfaces. We show that in the integral representation the complicated parameterization reduces to a decisive factor. We compare the natural and the characteristic subdivision finite element approach solving PDEs on surfaces. As model problem we consider the mean curvature flow, whereby the computation is done on the step-by-step changing geometry.

© 2016 Elsevier Ltd. All rights reserved.

1. Introduction

The subdivision surface concept came up with the idea of constructing smooth free-form surfaces by an iterative refinement of coarse control grids. A control grid is given by a polyhedral surface embedded in the Euclidean space \mathbb{R}^3 . It is the most basic geometric shape representation tool in modelling and engineering systems. The refinement is done step-by-step where the repeated application of subdivision rules to the emerging grid produces finer control grids that converge towards a smooth surface, called the limit surface. A single subdivision step can be written in matrix form obtaining the so called subdivision matrix. By means of the eigendecomposition of the subdivision matrix, we are able to evaluate the limit surface in given control grid vertices. In accordance to the used subdivision rules, the emerging limit surfaces characterize different classes of surfaces. For example, Lane and Riesenfeld [1] show that using weights from Pascal's

triangle produces piecewise B-spline surfaces of certain degree. However, one may have in mind that the existence of extraordinary vertices influences the smoothness of the limit surfaces. This has been extensively studied in [2,3]. Over the years, various subdivision schemes have been developed. For an overview of subdivision surfaces, we refer to Peters and Reif [4]; Cashman [5]; Ma [6].

To assemble the limit surface using subdivision might be a laborious process. By comparison, for some of the subdivision schemes, the limit surface has a piecewise parametric limit surface representation by which it can be computed in each point on the surface. In [7,8], Stam has introduced an exact evaluation scheme without any explicit subdivision of the initial control grid. Using discrete Fourier transform, an eigenstructure of the local subdivision matrix is obtained. In consequence of using Stam's idea, the labour-intensive subdivision process can be avoided, but with an undesirable side effect; the smoothness at the extraordinary vertices gets lost. Nevertheless, based on the underlying basis functions, the limit surface can be partitioned according to the control grid elements. A subdivision based finite element approach can be achieved. Such a construction has been firstly introduced to the area of engineering in [9]. Back then, it seemed to be promising. The artefacts related to the incorrect

[☆] This paper has been recommended for acceptance by Scott Schaefer and Charlie C.L. Wang.

^{*} Corresponding author.

E-mail address: anna.wawrzinek@fu-berlin.de (A. Wawrzinek).

integration over the irregular elements may not have been fully identified.

While performing numerical experiments of the convergence of natural subdivision finite elements difficulties have been encountered in [10]. Due to the unbounded estimates over irregular elements, the reason for the errors has been indicated in the incorrect use of the Gaussian quadrature. The defective integration has been also confirmed by the studies in [11]. The reason for this is the limit surface representation for irregular elements that is given by a piecewise polynomial function. At this point, the general Gaussian quadrature is therefore an inappropriate method for an exact approximation. In order to improve this, the piecewise evaluation up to a certain subdivision depth of the elements should be performed.

1.1. Contributions

In this paper, we introduce an isoparametric subdivision finite element approach that is consistent with the classical subdivision surfaces. This means that the presented shape functions maintain the C^1 -continuity at the irregular vertices. We give a precise definition of subdivision basis functions based on the Catmull–Clark subdivision. We distinguish between the natural and the characteristic parameterization of the limit surface. The last one ensures the smoothness of the classical defined subdivision surfaces, but the calculation is very expensive. We integrate the concept of element-based generating splines and isoparametric concept to obtain the corresponding finite element approaches. In addition, we derive the mass matrix and the stiffness matrix using the characteristic finite elements in greater detail. These are used for the integral representation of PDEs on subdivision surfaces. We show that the complex issue of deriving the inverse of the characteristic map reduces to an appropriate scaling factor in the integral representation.

As model problem, we investigate the mean curvature flow on closed subdivision surfaces. Therefore, the calculation is performed on a step-by-step evolving geometry. The introduced characteristic finite element improves the consistency of the subdivision control grid and, equivalently, of the limit surface. To verify this, we compare our result with the commonly used natural subdivision finite element.

1.2. Related work

Catmull–Clark subdivision surfaces [12] is one of the first and most commonly used subdivision schemes. In the limit of the subdivision, an almost everywhere C^2 -continuous surface is obtained, except the finite set of extraordinary vertices; but even there the normal continuity is ensured. In [8], an efficient evaluation of the limit surface is presented. Based on this, the so called natural parameterization is defined. However, Stam's parameterization results only in C^0 -continuity at the extraordinary vertices. To avoid this defect, a reparameterization based on the characteristic map can be used. Due to the computational effort, it does not seem to be feasible in practice [13]. On the other hand, the Catmull–Clark subdivision basis functions are square integrable [3] and therefore form a basis of the Sobolev space H^2 . This provides a solid foundation for a finite element construction.

A finite element discretization with subdivision surfaces has been introduced in [9,14,15]. Conforming Loop subdivision finite elements on triangular meshes has been used to discretize Kirchhoff–Love's type of thin shell model. An extension of the Catmull–Clark's subdivision scheme to volumetric solids and a corresponding finite element simulation of elastic bodies has been proposed by Burkhart et al. [16]. In [17], Koiter's thin shell model has been conforming discretized using Catmull–Clark

finite elements and applied to physical simulations, deformation-based modelling and calculation of free vibration modes. A numerical convergence analysis of this approach has been performed by Barendrecht [10]. Solving Poisson's equation on the disc, Nguyen et al. [11] present a classification of the Catmull–Clark finite elements according to several classical, discrete differential and isogeometric methods. In [18], adaptive isogeometric analysis is performed using truncated hierarchical Catmull–Clark subdivision splines. An isogeometric discretization approach to partial differential equations on Loop subdivision surfaces and a comparison of different quadrature schemes is discussed in [19]. Recently, Riffnaller-Schiefer et al. [20] have presented an extension subdivision based isogeometric analysis of the Kirchhoff–Love thin shell to NURBS compatible subdivision surfaces.

2. Generalized basis functions of Catmull–Clark type

One of the oldest subdivision schemes to iteratively generate smooth surfaces from coarse control grids is the Catmull–Clark scheme [12]. The scheme describes a generalization of tensor product bicubic B-splines to meshes with arbitrary topology. At each stage of the process, a control grid with quadrilateral connectivity is generated. The Catmull–Clark limit surface is an almost C^2 -continuous piecewise spline surface with singularities at the extraordinary vertices, i.e. vertices with valence unequal to four. Here, a singularity is a point where the general well-behaving differentiability fails.

In [8] a stable and efficient scheme has been introduced that allows for a direct evaluation of the limit surface at any point of the domain. The limit surface can be computed elementwise without any explicit subdivision of the control grid. Elementwise means that for each element of the grid a surface patch is obtained, with a smooth transition between the patches. For this purpose, the combinatorial connectivity of the one-ring of the element has to be examined. A one-ring of an element is the union of the element and the elements sharing at least one vertex with this element. Due to the connectivity, we distinguish two types of occurring elements, regular and irregular elements, and characterize the surface patches accordingly. If the element is regular, i.e., each vertex of the element has valence four, the corresponding surface patch is a bicubic B-spline patch. Otherwise, if one of the vertices is an extraordinary vertex, the element is called irregular. In this case, the surface patch is given by an infinite sequence of nested B-spline patches. We restrict ourselves to elements with at most one extraordinary vertex.

2.1. Natural generating spline

Given an arbitrary closed control grid $\mathcal{C}_\mathcal{Q}$. We consider an element $Q_c \subset \mathcal{C}_\mathcal{Q}$ and its one-ring. Using Stam's parameterization, we are able to derive the corresponding set of element-based basis functions.

Definition 2.1 (Natural Generating Spline). For an element Q_c of the Catmull–Clark grid $\mathcal{C}_\mathcal{Q}$, we consider the set of basis functions $\{b_j^* \mid j = 0, \dots, K-1\}$. The factor $K = 2\nu + 8$, where ν denotes the valence of the extraordinary vertex, describes the size of the set of vertices in the one-ring of Q_c . Let $b(u, v)$ be a vector, where the entries b_i , $i = 0, \dots, 15$ are the 16 uniform bicubic B-spline basis functions defined over the unit square $[0, 1]^2$. The natural generating spline is given by the vector

$$b^* = (b_0^*, b_1^*, \dots, b_{K-1}^*)^T,$$

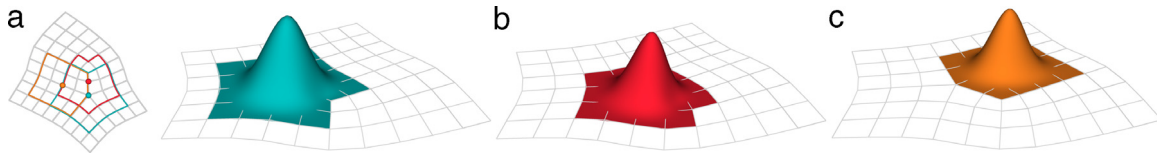


Fig. 1. Generalized B-spline basis functions corresponding to (a) an extraordinary vertex, (b) a regular vertex with at least one extraordinary vertex in its one-neighbourhood, and (c) a regular vertex without any extraordinary vertices in its one-neighbourhood. The last one is equivalent to a uniform bicubic B-spline basis function.

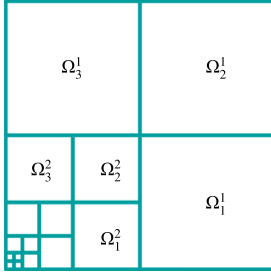


Fig. 2. Partition of the parameter domain $\Omega = [0, 1]^2$ into subdomains Ω_k^n .

where the entry b_j^* is described to be the j th basis function corresponding to the j th vertex in the one-ring of the element; it is defined by

$$b_j^* : \Omega \rightarrow \mathbb{R}$$

$$b_j^*(u, v) = \begin{cases} [S_{k,n}^T]_j b \circ t_{k,n}(u, v) & \text{for } (u, v) \in \Omega_k^n \\ b_j^\infty & \text{for } (u, v) = (0, 0), \end{cases} \quad (1)$$

for $n \geq 1$ and $k = 1, 2, 3$. $S_{k,n} = P_k S_n$ is given by the product of the subdivision matrix $S_n = \bar{A}A^{n-1}$, $n \geq 1$, and the picking matrix P_k , $k = 1, 2, 3$. For the parameter domain $\Omega = [0, 1]^2$, we consider the infinite partition of Ω into subdomains Ω_k^n shown in Fig. 2. The function $t_{k,n}$ describes the transformation from Ω_k^n to Ω . At the extraordinary vertex the value of the generalized basis function is given by the value b_j^∞ .

The term $[\cdot]_j$ denotes the j th row of the matrix. For the regular element, one of the regular vertices can be treated as extraordinary. Thus, $v = 4$ and the $K = 16$ basis functions of b^* are equivalent to the bicubic B-spline basis functions b_i in the irregular element ordering. If this is the case, for simplicity's sake, we evaluate the limit surface using the B-spline representation. Note, the parameter domain for both types of elements is the unit square. For details, see [8].

An one-neighbourhood of a vertex is the union of the elements that contain this vertex. A n -neighbourhood is the union of the $(n - 1)$ -neighbourhood and the elements that are sharing at least one vertex with the elements of the $(n - 1)$ -neighbourhood. To calculate b_j^∞ , we consider the classical limit surface evaluation scheme. Therefore, we examine the one-neighbourhood of the extraordinary vertex and assembly the corresponding subdivision matrix S . Note, the matrix S is stochastic and non-defective, i.e. it has a complete basis of eigenvectors. For each vertex v_j , $j = 0, \dots, a - 1$, in the one-neighbourhood we set up a control vertex position vector C_j where each entry is zero except for a one in the entry of the j th vertex. Consider the eigendecomposition of the subdivision matrix: The set $\Lambda = \{\lambda_k\}$ of ordered eigenvalues be given such that $\lambda_0 = 1 > \lambda_1 \geq \dots \geq \lambda_{a-1}$, a is the number of vertices in the one-neighbourhood. Let $\{v_k^r\}$ and $\{v_k^l\}$ be the sets of right and left eigenvectors, such that $v_0^r = (1, 1, \dots, 1)$ and $v_m^r \cdot v_n^l = \delta_{mn}$. The limit position of the basis function is given by

$$b_j^\infty = \lim_{n \rightarrow \infty} (S^n C_j)^T v_0^l = C_j^T v_0^l, \quad (2)$$

where v_0^l is the left eigenvector of S corresponding to the largest eigenvalue equal 1.

As aforementioned, each element-based basis function corresponds to a vertex in the one-ring of the element, and this, in turn, to a vertex in the control grid. Moreover, for each control vertex, we obtain a global basis function. This is described piecewise by the element-based basis functions. Due to the local dependence, the support of the global basis is prescribed to be the two-neighbourhood of a control vertex. Thus, for an element $Q_c \in \mathcal{C}_\mathcal{Q}$ in the two-neighbourhood of a vertex in the control grid, let this vertex correspond to the j th vertex in the one-ring of Q_c . The generating spline function b_j^* of Q_c describes then the parameterization of the global basis function associated with this vertex on the element Q_c . The global function is called the generalized B-spline basis function of Catmull–Clark type. It is known to be a bicubic polynomial on each regular patch or regular subpatch of the irregular element apart from the extraordinary vertex. We show examples of the possible emerging generalized B-spline basis functions in Fig. 1.

The emerging surface parameterization is called the natural parameterization. It is easy to use, but not fully compatible with the classical concept of subdivision surfaces. The defect of the parameterization is that the surface is only C^0 -continuous at the extraordinary vertices. In order to obtain a C^1 -parameterization, as in the classical concept, a suitable differentiable structure has to be put on the domain, or, equivalently, a suitable reparameterization of the basis functions has to be obtained.

2.2. Characteristic parameterization and its properties

We consider a fundamental concept of subdivision surfaces called the characteristic map. The characteristic map χ is very much linked to the subdivision matrix, i.e. it is defined by the two eigenvectors of the matrix that correspond to the subdominant eigenvalue λ [2,3]. Moreover, a subdivision scheme generates C^1 -continuous surfaces that are locally manifolds, if χ is regular and injective [2]. The continuity of the Catmull–Clark subdivision scheme has been proven in [21]. The image of the characteristic map is describing a two-dimensional spline domain in the plane, called the characteristic domain Ω_χ . The characteristic domain changes according to the valence of the extraordinary vertex. The characteristic domains for different vertex valences are shown in Fig. 3. Due to the injectivity of χ , we can think of a mapping $\chi^{-1} : \Omega_\chi \rightarrow \Omega$ as a parameterization of Ω . By the fact that χ is regular, i.e. χ has a non-singular Jacobian in the interior of each part of Ω . We consider the following reparameterization of the natural generating spline described in Definition 2.1.

Remark 2.1. Given an element $Q_c \subset \mathcal{C}_\mathcal{Q}$, we consider the associated generating spline b^* . Let χ be the corresponding characteristic map and $\Omega_\chi = \{(\xi, \eta) \in \mathbb{R}^2 \mid (\xi, \eta) = \chi(u, v), (u, v) \in \Omega\}$ be the characteristic domain. The components of the generating spline b^* can be reparameterized as follows

$$b_j^\chi : \Omega_\chi \rightarrow \mathbb{R}$$

$$b_j^\chi(\xi, \eta) = b_j^* \circ \chi^{-1}(\xi, \eta) \quad (\xi, \eta) \in \Omega_\chi, \quad (3)$$

where $j = 0, \dots, K - 1$ is the index of a vertex in the one-ring of Q_c . The basis function b_j^χ is at least C^1 -continuous for any $(\xi, \eta) \in \chi(\Omega)$ [2].

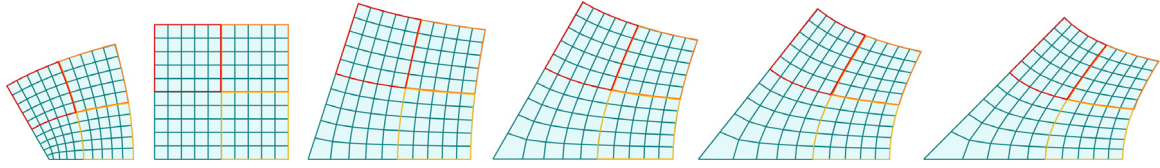


Fig. 3. Characteristic maps and segments for the vertex valence $v = 3, 4, 5, 6, 7, 8$. The blue patch is illustrating the map. The parts separated by the yellow, orange and red boundary are illustrating the characteristic domains $\Omega_\chi^{0,1}$, $\Omega_\chi^{1,1}$ and $\Omega_\chi^{2,1}$, respectively. (For interpretation of the references to colour in this figure legend, the reader is referred to the web version of this article.)

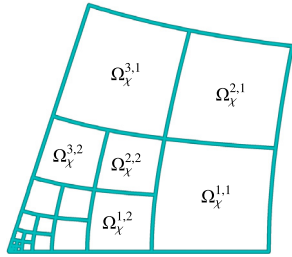


Fig. 4. Partition of the characteristic domain Ω_χ for a vertex of valence 5 into subdomains $\Omega_\chi^{k,n}$.

The given parameterization has been introduced in [2] for bivariate B-spline based subdivision surfaces. Moreover, it also has been considered in [22] for the proof of C^1 -continuity of general stationary subdivision surfaces. It is shown that χ puts a differentiable structure on the domain Ω . If χ and χ^{-1} exist everywhere, then a functional form of the representation can be derived. In the following, we consider the reparameterized basis functions for the definition of shape functions that preserve the C^1 -continuity at the extraordinary vertex.

We consider the piecewise representation of the characteristic map given by:

$$\chi : \Omega \rightarrow \mathbb{R}^2$$

$$\chi(u, v) = \begin{cases} \chi_{k,n} \circ t_{k,n}(u, v) & \text{for } (u, v) \in \Omega_k^n \\ (0, 0)^T & \text{for } (u, v) = (0, 0), \end{cases} \quad (4)$$

for

$$\chi_{k,n}(u, v) = \lambda^{n-1} (P_k \bar{A} V_\lambda)^T b(u, v) \quad (u, v) \in [0, 1]^2,$$

where the patches $\chi_{k,n} \circ t_{k,n}$ of the characteristic map are defined by means of the partitioned domain Ω . The map $t_{k,n}$ is the transformation of Ω_k^n into the B-spline domain $[0, 1]^2$, see Fig. 7. The matrix $V_\lambda = (v_1, v_2)$, called the subdominant matrix, is given by the two eigenvalues v_i , $i = 1, 2$, of the subdivision matrix A related to the subdominant eigenvalue λ . We obtain the partition of Ω_χ into subdomains $\Omega_\chi^{k,n}$, where $\Omega_\chi^{k,n}$ given through $\chi_{k,n}$ is describing the k th subpatch in the n th subdivision level of Ω_χ . Note, the partition of the characteristic domain Ω_χ and the partition of Ω are related, compare Figs. 4 and 2. Moreover, Ω is the characteristic domain Ω_χ of a vertex with valence four equivalent to a regular element. The partition of Ω_χ can be considered as an outcome of an ongoing subdivision of the resulting corner element that corresponds to the irregular element. Moreover, fixing a k , the domains $\Omega_\chi^{k,n}$ for $n \rightarrow \infty$ can be seen as scaled copies of each other in conformity with the origin $(0, 0) \in \Omega_\chi$. Three separate mappings can be determined.

Remark 2.2. Let $\chi_{k,n}$ be the mapping describing the subdomain $\Omega_\chi^{k,n}$. For a given $k, k = 1, 2, 3$, we obtain the mapping χ_k described by the relation

$$\chi_k : \Omega \rightarrow \mathbb{R}^2$$

$$\chi_k(u, v) = \lambda^{-n} \chi_{k,n}(u, v), \quad (5)$$

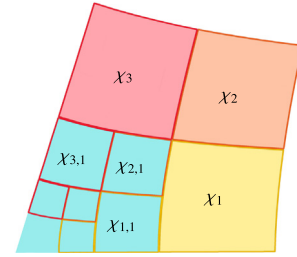


Fig. 5. Characteristic patches χ_k , $k = 1, 2, 3$. The scaled characteristic patches related to mappings $\chi_{k,n}$ are shown by the coloured frames in the characteristic domain Ω_χ (blue domain). (For interpretation of the references to colour in this figure legend, the reader is referred to the web version of this article.)

where χ_k defines one of the three extensions of the characteristic domain. The factor λ is given by the subdominant eigenvalue corresponding to the valence of the extraordinary.

Thus, the partition of the characteristic domain and the scaled patches characterize the mapping χ_k . Conversely, the mapping χ_k forms an initial module for the partition of Ω_χ :

Definition 2.2 (Characteristic Patches). By the use of the natural parameterization, the mapping χ_k , called the k th characteristic patch, can be defined by

$$\chi_k(u, v) = \bar{V}_\lambda^T P_k^T b(u, v) \quad (u, v) \in \Omega$$

where $\bar{V}_\lambda = \frac{1}{\lambda} \bar{A} V_\lambda$ describes an extension of the eigenvectors. The matrix \bar{A} is the extended subdivision matrix. The matrix $V_\lambda = (v_1, v_2)$ is the subdominant matrix.

The image of the characteristic patches has no overlap with the characteristic domain, except for the common boundary, see Fig. 5. Note, χ_k and χ are defined over the same domain Ω . The extension \bar{V}_λ of the eigenvectors relates to the extension of the characteristic patches χ_k . Moreover, the images of characteristic patches χ_k can be seen as the parameter domain in the characteristic domain of the corresponding three neighbouring elements in the control grid. The following relations between the characteristic mappings are valid:

Remark 2.3. The characteristic map χ fulfils the scaling relation

$$\chi(u/2, v/2) = \lambda \chi(u, v).$$

The characteristic patches χ_k , $k = 1, 2, 3$ fulfil the scaling relation

$$\lambda^n \chi_k(u, v) = \chi_{k,n}(u, v) = \chi_{k,n}, \quad (6)$$

for $n \geq 1$. Here, we consider the restriction of the characteristic map χ to the k th subpatch in the n th subdivision level of Ω_χ .

By means of the patchwise representation of the characteristic map, we define the characteristic generating spline by

Definition 2.3 (Characteristic Generating Spline). Given an element $Q_c \subset \mathcal{C}_Q$. Let χ be the corresponding characteristic map described by the patchwise representation as in Eq. (4). Thus, we consider the

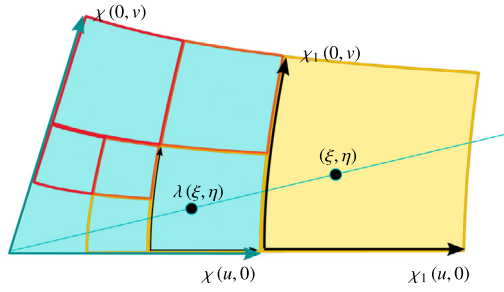


Fig. 6. Schematic illustration of the scaling relation. The point $(\tilde{\xi}, \tilde{\eta}) = \lambda(\xi, \eta) \in \Omega_\chi$ is given by the scaling of $(\xi, \eta) \in \chi_1(\Omega)$.

partition of Ω_χ into the subdomains $\Omega_\chi^{k,n}$. The components of the generating spline b^χ can be reparameterized by

$$b_j^\chi : \Omega_\chi \rightarrow \mathbb{R}$$

$$b_j^\chi(\xi, \eta) = \begin{cases} [S_{k,n}^T]_j b \circ \chi_{k,n}^{-1}(\xi, \eta) & \text{for } (\xi, \eta) \in \Omega_\chi^{k,n} \\ b_j^\infty & \text{for } (\xi, \eta) = (0, 0) \end{cases} \quad (7)$$

where b_j^χ are the components of the characteristic generating spline

$$b^\chi = (b_0^\chi, b_1^\chi, \dots, b_{K-1}^\chi)^T.$$

The term $[\cdot]_j$ denotes the restriction to the j th row of the matrix.

In contrast to the parameterization over Ω , the reparameterization over the characteristic domain Ω_χ provides the desired compatibility with the classical subdivision surface continuity, i.e. the C^1 -continuity at the extraordinary vertex is preserved.

According to the reparameterization, we sum up the properties of the transformation from Ω_χ to the subdomains $\Omega_\chi^{k,n}$. We write here $(\tilde{\xi}, \tilde{\eta}) = \chi(\tilde{u}, \tilde{v})$ for the coordinates of a point in the domain Ω_χ and $(\xi, \eta) = \chi_k(u, v)$ for the coordinates in the image of the characteristic patch χ_k . We choose a point $(\tilde{\xi}, \tilde{\eta}) \in \Omega_\chi$, such that $(\tilde{\xi}, \tilde{\eta}) = \lambda^n(\xi, \eta)$. Using the scaling relation, see Eq. (6), we know that such a point exists. For a schematic illustration, see Fig. 6. Considering the change of coordinates from Ω_χ to $\Omega_\chi^{k,n}$, we have:

$$\chi^{-1}(\tilde{\xi}, \tilde{\eta}) = \chi^{-1}(\lambda^n \xi, \lambda^n \eta) = \chi_{k,n}^{-1}(\xi, \eta), \quad (8)$$

where the scaling is proportional to the level of subdivision of the characteristic domain. The reparameterization by $\chi_{k,n}^{-1}$ instead of χ^{-1} means to substitute $(\lambda^n \xi, \lambda^n \eta)$ where $(\xi, \eta) \in \chi_{k,n}(\Omega)$.

The Jacobian of the transformation of the coordinates is obtained by

$$J_\chi = \frac{\partial(\tilde{\xi}, \tilde{\eta})}{\partial(\xi, \eta)} = \lambda^n I, \quad (9)$$

where I denotes the identity matrix. The Jacobian is constant, i.e. the transformation is invertible. Now, we restrict the gradient ∇_χ over the domain $\Omega_\chi = \chi(\Omega)$ to the subdomain $\Omega_\chi^{k,n} = \chi_{k,n}(\Omega)$.

Remark 2.4. The gradient ∇_χ restricted to $\Omega_\chi^{k,n}$ is given by

$$\nabla_\chi|_{\Omega_\chi^{k,n}} = \lambda^{-n} \nabla_{\chi_{k,n}},$$

where $\nabla_{\chi_{k,n}}$ is the surface gradient over $\Omega_\chi^{k,n}$.

This follows directly from differentiating Eq. (8).

3. The isoparametric Catmull–Clark finite element approach

Given an arbitrary control grid, we consider a unique Catmull–Clark limit surface together with an elementwise parameterization. An interplay between two meshes is described, the control grid and the physical mesh. The control grid can be seen as a scaffold of the physical mesh. Here, we will restrict ourselves to closed limit surfaces, such that for each control grid element a complete one-ring can be determined. According to the parameterization, the surface is described by a patchwork of glued together surface patches, i.e. we obtain for each element of the control grid one surface patch. In turn, for each patch a set of basis functions is determined from the generating spline. This allows for a finite element construction.

In the previous section, two generating splines have been discussed for the elementwise parameterization of the Catmull–Clark limit surface, the natural and the characteristic generating spline. It is shown that for the natural one the smoothness lacks at the singularities, in contrast to the characteristic spline that preserves the smoothness. Therefore, two finite element approaches can be obtained with the corresponding quality. The natural approach has already been well established in the literature [17,10,11]. Using the characteristic spline, we introduce an isoparametric finite element approach that is consistent with the classical subdivision surfaces. Furthermore, the characteristic finite element is at least $C^1 \cap H^2$ everywhere. Based on this, a conforming finite element approach for PDEs up to fourth order is obtained.

3.1. Catmull–Clark finite elements

Let \mathcal{Q} be a smooth subdivision limit surface with the corresponding control grid $\mathcal{C}_\mathcal{Q}$, both immersed in \mathbb{R}^3 . The limit surface is described to be a generalized B-spline surface, i.e. the set of global basis functions of the surface is given by the underlying set of generalized B-splines corresponding to the vertices of the grid. We obtain the physical grid described by the surface patches $Q \subset \mathcal{Q}$ corresponding to the elements Q_c of the control grid $\mathcal{C}_\mathcal{Q}$. For each patch Q or, equivalently, each element Q_c , a set of element-based basis functions is given by the generating spline. As aforementioned, these element-based functions describe the piecewise parameterization of the generalized B-splines.

By means of the natural parameterization, the surface patch Q is defined by the function $s_Q : \Omega \rightarrow \mathbb{R}^3$ over the reference domain Ω , such that

$$s_Q(u, v) = \sum_j c_j b_j^*(u, v), \quad (u, v) \in \Omega,$$

where c_j is the position of the j th control vertex in the one-ring of the appropriate element $Q_c \subset \mathcal{C}_\mathcal{Q}$. Due to the partition of Ω , we can also use the patchwise representation $s_Q(u, v)|_{\Omega_k^n} = s_{k,n} \circ t_{k,n}(u, v)$, for details see [8]. The limit surface \mathcal{Q} is therefore given by the union

$$\mathcal{Q} := \bigcup_Q s_Q(\Omega)$$

of all surface patches Q . We consider the transformation of the reference domain Ω to the corresponding characteristic domain Ω_χ by the characteristic map χ . Moreover, the surface patch Q can be parameterized by the natural mapping $s_Q(\Omega)$ and the characteristic mapping $s_Q \circ \chi^{-1}(\Omega_\chi)$. If the control grid element Q_c is regular, then both surface parameterizations are equivalent to the B-spline representation with the uniform bicubic basis b , see Definition 2.1.

For an isoparametric approach, the same basis functions are used for the definition of the shape functions in the solution space as for the representation of the surface. We consider six different notions of element-based basis functions. Depending on the domain, we distinguish between:

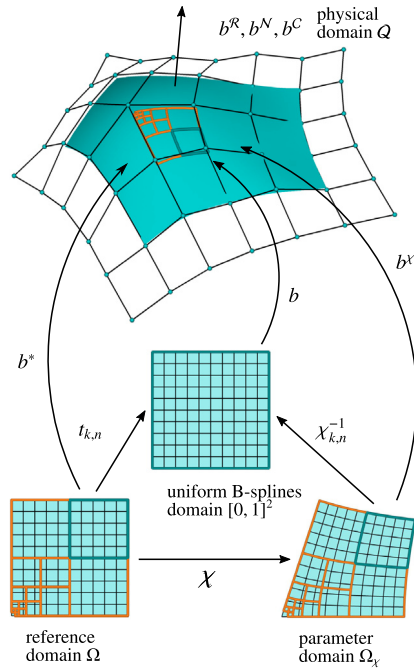


Fig. 7. Schematic illustration of the domains and the corresponding basis functions.

- the uniform B-spline basis b on $[0, 1]^2$,
- the regular shape functions b^R on a regular patch Q
- the natural generating spline basis b^* on the reference domain $\Omega = \bigcup \Omega_k^n$,
- the natural shape functions b^N on an irregular patch Q
- the characteristic generating spline basis b^x on the characteristic domain Ω_χ ,
- and, the characteristic shape functions b^c on an irregular patch Q .

The particular basis functions are illustrated in Fig. 7. The shape functions b^R , b^N and b^c on the surface are obtained by the pullback of the generating spline b , b^* and b^x , respectively, by the surface patch parameterization s_Q . In the following, we want to define the characteristic finite element approach. Therefore, the characteristic parameterization of the surface is obtained over the characteristic domain.

Definition 3.1 (Characteristic Finite Element). The isoparametric shape function $b^c : Q \rightarrow \mathbb{R}$ is defined over each surface element $Q \subset \mathcal{Q}$ separately by the bullbacks of the characteristic generating spline

$$b^c(p) = b^x \circ \chi \circ s_Q^{-1}(p) \tag{10}$$

where $p = s_Q(u, v) \in Q$ for $(u, v) \in \Omega$. The function space over the surface patch Q is given by

$$S_h^Q = \{x_Q \in \text{span}\{b_i^c\}\},$$

the span of the set of shape functions $b_i^c \in b^c$.

Due to the continuity of basis functions, the function space over the surface \mathcal{Q} is given by the union

$$S_h = \bigcup_Q S_h^Q = \left\{ x = \bigcup_Q x_Q \mid x_Q \in S_h^Q \right\} \tag{11}$$

of the subspaces S_h^Q over the surface patches $Q \subset \mathcal{Q}$. Additionally, we distinguish between regular and irregular elements, i.e.

$$S_h = \bigcup_{Q \text{ reg}} S_h^Q \cup \bigcup_{Q \text{ irreg}} S_h^Q$$

where for the regular elements the subspaces

$$S_h^Q = \{x_Q \in \text{span}\{b_i^R\}\} \quad \text{if } Q \text{ reg}$$

are given by the span of the regular shape functions b^R .

3.2. Derivatives on surfaces

Here, we briefly summarize some concepts relevant for the calculation of integrals over surfaces. Applying this, all concepts have to be adjusted to the appropriate domain. For a general definition, we consider a mapping $s : \Omega \subset \mathbb{R}^2 \rightarrow \mathbb{R}^3$ which takes as input the vector $(u, v) \in \Omega$ and produces as output the vector $s(u, v) \in \mathbb{R}^3$. The Jacobian matrix is described by

$$J_s = (s_{,u} \ s_{,v}),$$

where the entries $s_{,w}$, for $w \in \{u, v\}$, are column vectors described by the tangent vectors

$$s_{,w} = \frac{\partial s(u, v)}{\partial w},$$

given by the partial derivatives of the surface mapping. By $G_s = J_s^T J_s$ we denote the first fundamental form of s . The Jacobian determinant $|J_s|$ is defined by

$$|J_s| = \sqrt{\det(G_s)}.$$

It describes the change of the area in the area element. The area element of s is defined by $ds = |J_s| \, du \, dv$.

To deal with different variational forms, derivatives of functions defined on the mapping s have to be obtained. Is J_s the Jacobian of s , such that G_s is invertible, then the product

$$J_s^\dagger = G_s^{-1} J_s^T$$

is called the Moore–Penrose pseudo-inverse of J_s . A pseudo-inverse describes the generalization of an inverse matrix for singular and non-quadratic matrices. Let $f : \mathbb{R}^3 \rightarrow \mathbb{R}$ be a mapping defined on the surface s . The surface gradient $\nabla_{\mathcal{Q}} f$ is defined by

$$\nabla_{\mathcal{Q}} f(p) = (J_s^\dagger)^T \nabla (f \circ s)(u),$$

for $p = s(u, v)$ and $(u, v) \in \Omega$, where the vector

$$(\nabla (f \circ s))^T = \left(\frac{\partial f(s(u, v))}{\partial u}, \frac{\partial f(s(u, v))}{\partial v} \right) \in \mathbb{R}^2$$

is describing the common gradient of the function f . Note, the surface gradient $\nabla_{\mathcal{Q}} f$ depends on the parameterization of the surface s .

3.3. Integrals over smooths limit surfaces

In this section, we derive the formulas of two general integrals over the Catmull–Clark surface \mathcal{Q} . The formulas serve as a basis framework for the assembly of the variational formulations of different PDEs up to second order, but an extension to order four can be achieved using the forthcoming definition of the surface gradient.

We consider the integral of the product of two shape functions b^c over the surface \mathcal{Q} that is the ij th entry of the mass matrix

$$M_{ij} = \int_{\mathcal{Q}} b_i^c b_j^c \, d\mathcal{Q}$$

and the integral of the scalar product of the surface gradients of two basis functions that is the ij th entry of the stiffness matrix

$$D_{ij} = \int_{\mathcal{Q}} (\nabla_{\mathcal{Q}} b_i^c)^T \nabla_{\mathcal{Q}} b_j^c \, d\mathcal{Q}.$$

By the definition of basis functions, we consider an elementwise assembling, i.e. the integral over the surface \mathcal{Q} splits into integrals over the surface patches $Q \subset \mathcal{Q}$. As it is a common practice in finite element method, a pull-back of the integrated patch to the reference domain is obtained.

For simplicity's sake, we distinguish between the regular and the irregular element. For $Q \subset \mathcal{Q}$, if the corresponding control grid element is Q_c regular, then the reference domain is the B-spline domain $[0, 1]^2$. Moreover, the generating spline $b^\chi = b^* = b$ is given by the 16 bicubic B-spline basis functions. We consider the regular shape functions $b_j^R : Q \rightarrow \mathbb{R}$, $j = 0, \dots, 15$, over Q given by the composition

$$b_j^R := b_j \circ s_Q^{-1},$$

where $b_j : \Omega \rightarrow \mathbb{R}$ is the j th uniform B-spline basis function corresponding to the j th vertex in the one-ring of the element. Using the usual change of coordinates, the ij th entry M_{ij}^Q of the mass matrix over Q can be calculated from the formula

$$M_{ij}^Q = \int_{[0,1]^2} b_i b_j |J_{s_Q}| \, dudv, \quad (12)$$

where J_{s_Q} is the Jacobian of the transformation s_Q and $|J_{s_Q}|$ is the Jacobian determinant. For the ij th entry D_{ij}^Q of the stiffness matrix we can write

$$D_{ij}^Q = \int_{[0,1]^2} (\nabla b_i)^T G_{s_Q}^{-T} \nabla b_j |J_{s_Q}| \, dudv. \quad (13)$$

The term $G_{s_Q}^{-T}$ is the transposed inverse of the first fundamental form G_{s_Q} of the surface patch s_Q .

For $Q \subset \mathcal{Q}$, if the corresponding control grid element Q_c is irregular, then the parameter domain of the corresponding patch Q is given by the characteristic domain Ω_χ that is depending on the valence of the irregular vertex. The shape functions b^c are defined by the push-forwards of the characteristic generating spline functions

$$b_j^c := b_j^\chi \circ \chi \circ s_Q^{-1}, \quad (14)$$

where $s_Q \circ \chi^{-1}$ is the reparameterization of the surface patch Q to the domain Ω_χ . For the basis functions $b_j^\chi : \Omega_\chi \rightarrow \mathbb{R}$ we consider the patchwise formulation as defined in Eq. (7)

$$b_j^\chi(\xi, \eta) = [S_{k,n}^T]_j b \circ \chi_{k,n}^{-1}(\xi, \eta), \quad (\xi, \eta) \in \Omega_\chi^{k,n}. \quad (15)$$

In order to avoid the restriction $[S_{k,n}^T]_j$ to the rows of the matrix, we obtain the element mass matrix M^Q . This can be calculated as follows.

Theorem 3.1. *Let Q be a surface patch corresponding to an irregular control grid element. Using the isoparametric characteristic approach, the element mass matrix M^Q is given by the sum*

$$M^Q = \lim_{n \rightarrow \infty} \sum_{k,n} S_{k,n}^T M^{k,n} S_{k,n}$$

where $S_{k,n} = P_k S_n$ is the subdivision matrix that localizes the k th subpatch in the n th subdivision level. The matrix $M^{k,n}$ is the mass matrix of the subpatch $s_{k,n} \in Q$. Its entries are given by

$$M_{\alpha\beta}^{k,n} = \int_{[0,1]^2} b_\alpha b_\beta |J_{s_{k,n}}| \, dudv, \quad (16)$$

where b_γ is the γ th uniform B-spline basis function, for $\gamma = 0, \dots, 15$.

The matrix $M^{k,n}$ is a 16×16 -matrix corresponding to the vertices in the one-ring of an element that results from the subdivision with matrix $S_{k,n}$. Applying the subdivision matrix $S_{k,n}$ to the matrix $M^{k,n}$ will distribute the entries to the degrees-of-freedom of patch Q corresponding to the appropriate vertices in the one-ring of the element Q_c .

Proof. Let b_i^c and b_j^c be two shape functions described over the surface patch Q . The integral of the product of these functions over Q is defined by

$$M_{ij}^Q = \int_Q b_i^c b_j^c \, dQ$$

The function b_i^c fulfils the composition $b_i^c(q) = b_i^\chi \circ \chi \circ s_Q^{-1}(q)$ for $q \in Q$, such that $b_i^c(q) = b_i^\chi(\xi)$ for $\xi \in \Omega_\chi$. Using the chain rule $(s_Q \circ \chi^{-1})'(\xi) = s_Q'(\chi^{-1}(\xi))(\chi^{-1})'(\xi)$ it holds that

$$= \int_{\Omega_\chi} b_i^\chi b_j^\chi |J_{s_Q \circ \chi^{-1}}| \, d\Omega_\chi$$

where $J_{s_Q \circ \chi^{-1}} = J_{s_Q} J_{\chi^{-1}}$ and $J_{s_Q} = (s_{Q,1} s_{Q,2})|_{\chi^{-1}(\xi)}$, for $J_{\chi^{-1}}$ see Eq. (9). Consider the infinite partition of Ω_χ into $\Omega_\chi^{k,n}$, see Fig. 4. Using the restrictions to $\Omega_\chi^{k,n}$, we have

$$= \lim_{n \rightarrow \infty} \sum_{k,n} \int_{\Omega_\chi^{k,n}} (b_i^\chi \circ \iota_{k,n}) (b_j^\chi \circ \iota_{k,n}) |J_{s_Q \circ \chi^{-1}}| \circ \iota_{k,n} \\ \times |J_{\iota_{k,n}}| \, d\Omega_\chi^{k,n}$$

where $\iota_{k,n}$ is the identity map restricting to the domain $\Omega_\chi^{k,n}$, with $|J_{\iota_{k,n}}| = 1$. Using the patchwise parameterization $s_Q|_{\Omega_\chi^{k,n}} \circ \chi^{-1} = s_{k,n} \circ \iota_{k,n} \circ \chi^{-1}$ of the surface s_Q , the restriction to $\Omega_\chi^{k,n}$ is given by $s_Q \circ \chi^{-1} \circ \iota_{k,n} = s_{k,n} \circ \chi_{k,n}^{-1}$. The restriction of the Jacobian determinant results in $|J_{s_Q \circ \chi^{-1}}| \circ \iota_{k,n} = |J_{s_{k,n} \circ \chi_{k,n}^{-1}}|$. The basis functions are obtained by $b_i^\chi \circ \iota_{k,n} = [S_{k,n}^T]_i b \circ \chi_{k,n}^{-1}$. Hence, we consider the infinite sum

$$= \lim_{n \rightarrow \infty} \sum_{k,n} [S_{k,n}]_i^T M_\chi^{k,n} [S_{k,n}]_j$$

with the matrix $M_\chi^{k,n}$, where the entries $(M_\chi^{k,n})_{\alpha\beta}$ are defined by

$$(M_\chi^{k,n})_{\alpha\beta} = \int_{\Omega_\chi^{k,n}} (b_\alpha \circ \chi_{k,n}^{-1}) (b_\beta \circ \chi_{k,n}^{-1}) |J_{s_{k,n} \circ \chi_{k,n}^{-1}}| \, d\Omega_\chi^{k,n}.$$

Now, we transform $\Omega_\chi^{k,n}$ to the B-spline domain $[0, 1]^2$ by $\chi_{k,n}$. Due to the chain rule, we obtain

$$= \lim_{n \rightarrow \infty} \sum_{k,n} [S_{k,n}^T]_i M^{k,n} [S_{k,n}]_j$$

with the matrix $M^{k,n}$. The entries $M_{\alpha\beta}^{k,n}$ are given as in Eq. (16). \square

The integrand is therefore pulled back to the B-spline domain $[0, 1]^2$ by taking a detour through the parameter domain Ω_χ , where the partition into the subdomains $\Omega_\chi^{k,n}$ is considered.

Theorem 3.2. *Let Q be a surface patch corresponding to an irregular control grid element. Let λ be the subdominant eigenvalue of the subdivision matrix of the corresponding control element. Considering the characteristic generating spline, the surface gradient ∇_Q of the function b_i^c is patchwise described over the unit square by*

$$\nabla_Q b_i^c|_{s_{k,n}} = \lambda^{-n} \left([S_{k,n}^T]_i \nabla b(u, v) J_{s_{k,n}}^\dagger \right)^T \quad (u, v) \in [0, 1]^2$$

where $|_{s_{k,n}}$ denote the restriction to the subpatch $s_{k,n}$. The term $\nabla b(u, v)$ be given by the 16×2 -matrix of the componentwise evaluation of the gradient of the vector entries $b_j(u, v)$, such that each entry $\nabla b_j(u, v)$ is a 1×2 vector of the partial derivatives of b_j . The term $J_{s_{k,n}}^\dagger$ denote the Moore–Penrose inverse of the surface patch $s_{k,n}$.

The surface gradient is constituted patchwise by the pull-backs of the surface patches $s_{k,n}$ to the B-spline domain $[0, 1]^2$.

Proof. We consider

$$\nabla_Q b_i^c = \nabla_Q (b_\chi^i \circ \chi \circ s_Q^{-1})$$

The function b_i^c fulfils the composition $b_i^c(q) = b_\chi^i \circ \chi \circ s_Q^{-1}(q)$ for $q \in Q$, such that $b_i^c(q) = b_\chi^i(\xi)$ for $\xi \in \Omega_\chi$. Using the Chain rule, we have

$$= (J_{s_Q \circ \chi^{-1}}^\dagger)^T \nabla_\chi b_\chi^i$$

the transformation to the characteristic domain Ω_χ . The term $J_{s_Q \circ \chi^{-1}}$ is the Moore–Penrose inverse of $s_Q \circ \chi^{-1}$. We consider the partition of Ω_χ and restrict the parameterization to the corresponding subpatches $\Omega_\chi^{k,n}$

$$(J_{s_Q \circ \chi^{-1}}^\dagger)^T \nabla_\chi b_\chi^i \Big|_{\Omega_\chi^{k,n}} = (J_{s_Q \circ \chi^{-1}}^\dagger)^T \circ \iota_{k,n} \nabla_\chi b_\chi^i \circ \iota_{k,n}$$

where $\iota_{k,n}$ is the identity mapping, such that $|J_{\iota_{k,n}}| = 1$. By Remark 2.4, we can write

$$= (J_{s_{k,n} \circ \chi_{k,n}^{-1}}^\dagger)^T \lambda^{-n} \nabla_{\chi_{k,n}} [S_{k,n}^T]_i b \circ \chi_{k,n}^{-1}$$

hence, we consider the transformation to the B-spline domain $[0, 1]^2$, such that

$$= \lambda^{-n} (J_{s_{k,n}}^\dagger)^T ([S_{k,n}^T]_i \nabla b)^T.$$

This yields directly the assumption, where the pullback of the subpatch $s_{k,n}$ to the B-spline domain $[0, 1]^2$ is described. Due to the patchwise parameterization $s_{k,n}$ of the surface patch s_Q , the restriction of $\nabla_Q b_i^c$ to $\Omega_\chi^{k,n}$ is given by $s_{k,n} \circ \chi_{k,n}^{-1}$. \square

We consider the following definition for the element stiffness matrix:

Theorem 3.3. Let Q be a surface patch corresponding to an irregular control grid element. Using the isogeometric approach, the integral of the product of the surface gradients of the shape functions b_i^c and b_j^c can be obtained over the B-spline domain $[0, 1]^2$ by the element stiffness matrix

$$D^Q = \lim_{n \rightarrow \infty} \sum_{k,n} \lambda^{-2n} S_{k,n}^T D^{k,n} S_{k,n}$$

where $S_{k,n} = P_k S_n$ is the subdivision matrix that localizes the k th subpatch in the n th subdivision level. The matrix $D^{k,n}$ is the stiffness matrix of the subpatch $s_{k,n} \in Q$. The entries are defined by

$$D_{\alpha\beta}^{k,n} = \int_{[0,1]^2} (\nabla b_\alpha)^T G_{s_{k,n}}^{-T} \nabla b_\beta |J_{s_{k,n}}| dudv \quad (17)$$

where ∇b_γ is the gradient of the γ th uniform B-spline basis function, for $\gamma = 0, \dots, 15$. The term $G_{s_{k,n}}$ is the first fundamental form of the subpatch $s_{k,n}$.

Proof. For the representation of the integral over the B-spline domain $[0, 1]^2$, we use Theorem 3.2. Therefore, we can skip the intermediate steps as in the proof of Theorem 3.1 and write

$$D_{ij}^Q = \int_Q (\nabla_Q b_i^c)^T \nabla_Q b_j^c dQ$$

transposing and using the definition of the Moore–Penrose inverse, we have

$$= \lim_{n \rightarrow \infty} \sum_{k,n} \lambda^{-2n} \int_{[0,1]^2} [S_{k,n}^T]_i \nabla b G_{s_{k,n}}^{-T} ([S_{k,n}^T]_j \nabla b)^T \times |J_{s_{k,n}}| dudv$$

The rows of ∇b are given by the transpose of the gradients ∇b_γ

$$= \lim_{n \rightarrow \infty} \sum_{k,n} [S_{k,n}^T D^{k,n} S_{k,n}]_{ij}$$

with the matrix $D^{k,n}$ with the entries $D_{\alpha\beta}^{k,n}$ given as in Eq. (17). \square

4. Applications

In this section, we apply the elaborated results to a geometric PDE problem on Catmull–Clark limit surfaces. As model problem we consider the mean curvature flow. Due to the non-trivial treatment of boundary conditions for the subdivision surface framework, which have not been taken into consideration in this work, we limit the applications to closed surfaces.

4.1. Mean curvature flow

Let \mathcal{Q}_0 be a compact orientable two-dimensional surface smoothly embedded in \mathbb{R}^3 which is locally given by the mapping $x_0 : \Omega \rightarrow \mathbb{R}^3$, where $\Omega \subset \mathbb{R}^2$ and $x_0(\Omega) \subset \mathcal{Q}_0$. Our intention is to find the family $\{x : (\cdot, t) \Omega \rightarrow \mathbb{R}^3 \mid t > 0\}$ of mappings such that

$$\frac{\partial x}{\partial t}(u, t) = \Delta_{\mathcal{Q}(t)} x(u, t) \quad x(u, t) \in \Omega \times I \quad (18)$$

$$x(\cdot, 0) = x_0(\cdot),$$

where $I = (0, T)$, for some $T > 0$. The term $\Delta_{\mathcal{Q}(t)}$ describes the Laplace–Beltrami operator on $\mathcal{Q}(t)$. Here $\mathcal{Q}(t)$ is the surface given locally by the mapping $x(\Omega, t) \subset \mathcal{Q}(t)$. Thus, we consider the identity $x(\cdot, t) := id_{\mathcal{Q}(t)}$.

We are interested in a discretized representation of this initial-value problem. The space and time variables are decoupled and can be treated independently. We consider therefore the Rothe’s method, where we first resolve the time, then the space problem. To ensure the stability, we use for the time discretization the backward Euler method. Let $\tau > 0$ be a discrete time such that $t_k = t_0 + k\tau$, $k = 0, 1, \dots$, is an equidistant time partition. We assume $t_0 = 0$. For all k , let x^{k+1} be the mapping that parameterizes a smooth surface $\mathcal{Q}_{k+1} = \{x^{k+1}(u) \mid u \in \mathcal{Q}_k\}$ over \mathcal{Q}_k . A time discretized form of Eq. (18) is given by

$$x^{k+1}(u) - \tau \Delta_{\mathcal{Q}_k} x^{k+1}(u) = x^k(u) \quad u \in \mathcal{Q}_k \quad (19)$$

$$x^0(\Omega) \in \mathcal{Q}_0,$$

where $x^{k+1} : \mathcal{Q}_k \rightarrow \mathcal{Q}_{k+1}$ and \mathcal{Q}_0 is a given initial configuration defined over Ω . Therefore, we obtain at each time step an elliptic boundary value problem.

Now, we transform the problem from Eq. (19) into the corresponding weak formulation. It is a common practice in the classical finite element method to use the flow in practice. Given an initial surface \mathcal{Q}_0 :

Problem 4.1. Find $x^{k+1}(\cdot) : \mathcal{Q}_k \rightarrow \mathbb{R}^3$, such that for all $\varphi \in S_h$:

$$\int_{\mathcal{Q}_k} x^{k+1} w \, d\mathcal{Q} + \tau \int_{\mathcal{Q}_k} \nabla_{\mathcal{Q}_k} x^{k+1} \nabla_{\mathcal{Q}_k} w \, d\mathcal{Q} = \int_{\mathcal{Q}_k} x^k w \, d\mathcal{Q}$$

for all $w \in S_h(\mathcal{Q}_k)$ with $x^{k+1} \in S_h(\mathcal{Q}_k)$, where $x^k = id_{\mathcal{Q}_k}$. The term $\nabla_{\mathcal{Q}_k}$ denotes the surface gradient over $\nabla_{\mathcal{Q}_k}$.

The approximate solution x^{k+1} of the weak problem is considered in a subspace of the space H^1 .

Catmull–Clark limit surfaces are H^2 -regular, the finite element space $S_h(\mathcal{Q}_k)$ we constructed, see Formula (11), is therefore a subspace of the Sobolev space $H^2 \subset H^1$. Thus, we consider a conforming discretization of the mean curvature flow. Let $\{x_j^k\}$ be the set of coefficients corresponding to the vertices of the control grid of surface \mathcal{Q}_k . For each of the vertices x_j^k we consider the corresponding generalized B-spline basis function. Note, the restriction of the generalized B-spline to a control grid element is described by the corresponding function b^e , see Formula (10). Using the patchwise representation

$$x^k = \bigcup_Q \sum_j x_j^k b_j^e(q) \quad q \in Q$$

with the coefficients x_j^k , for a fixed time $\tau > 0$, we rewrite the problem into the linear system

$$(M + \tau D) X^{k+1} = M X^k, \quad (20)$$

where the i th entry of the coefficient vector X^k is given by x_i^k . As described in Section 3.3, the mass matrix M and the stiffness matrix D are patchwise evaluated using the integrals M^Q and D^Q , respectively. Note, the Jacobian matrix and determinant are non-linear and vary from patch to patch.

4.2. Experiments

To solve Problem 4.1 over an arbitrary limit surface, we have to use a numerical quadrature approach. The Gaussian quadrature is a quadrature method known for the exact integration of polynomial functions up to a prescribed degree. Integration of square elements can be done by using the tensor product of the one-dimensional formula. Here, the notation “ a^2 ” means we apply a points in each directions that provide a^2 evaluation points for each integral. Considering Eqs. (16) and (17), the functions to be integrated are non-polynomial functions. This is due to the occurrence of the non-constant Jacobian determinant $|J|$ and the inverse of the first fundamental form G^{-1} . Therefore, an exact integration cannot be achieved. Due to Strang’s Lemma, an exact is not needed to obtain the optimal convergence rate of finite element solutions, see [23, Ch. 4]. In particular, the quadrature error has to preserve the interpolation error. Hence, an integration scheme for non-polynomial functions is needed.

For the calculation, we keep the current distinction between regular and irregular elements. On a regular patch, the shape functions b^e are given by polynomials of bi-degree 3. Therefore, the evaluation of the integral over the patch is done in one go. For an irregular element, the shape functions b^e are piecewise polynomials of bi-degree 3. We have to apply the Gaussian quadrature to each of the summands of the integral, see Theorems 3.1 and 3.3. Due to the infinite sum, we have to be satisfied with an another approximation and apply the Gaussian quadrature to each subintegral up to a prescribed subdivision level. In [11], the authors have shown that an evaluation up the level $n = 7$ is necessary to stabilize the results. In the following, we will decide experimentally on the choice of quadrature rule.

In the first experiment, we consider a control grid with only regular elements whose points lie on a torus, see Fig. 8. We

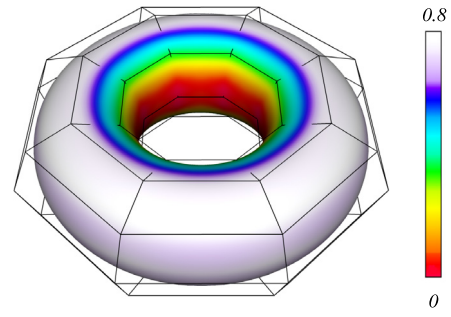


Fig. 8. The control grid and the limit surface of the torus model. The colouring of the limit surface is given by the mean curvature of the limit surface. (For interpretation of the references to colour in this figure legend, the reader is referred to the web version of this article.)

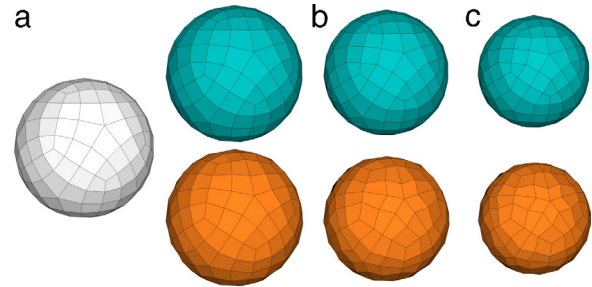


Fig. 9. The mean curvature flow using different shape function representations: the characteristic shape functions (blue) and the natural shape function (orange). The initial grid is shown in white. The flow of time (a) t_1 , (b) t_5 and (c) t_{10} for the time step size $\tau = 0.1$. (For interpretation of the references to colour in this figure legend, the reader is referred to the web version of this article.)

examine the model to find a proper justification for the choice of subdivision level and the number of Gaussian quadrature knots for the evaluation of the problem matrices. We assemble the mass and the stiffness matrix of the model using both: the regular element evaluation obtained by Formula (12) and the irregular element evaluation described in Theorem 3.1. The piecewise quadrature has been done for different subdivision levels. To verify the results we calculate the row-sum norm and the Frobenius norm of the matrices using the 2^2 -, 3^2 - and 4^2 -point Gaussian quadrature. In Tables 1 and 2, we show the comparison of the matrix norms of the evaluated mass and stiffness matrices. Therefore, we decide to use the 4^2 -point quadrature on regular elements, and the 3^2 -points for the piecewise quadrature on irregular elements. Additionally, we choose the 9th subdivision level as a reference.

In the second experiment, we consider a control grid, which points lie on a sphere. The control grid is derived from a twice subdivided icosahedron, where the control points of the grid have been projected to the unit sphere. Due to the properties of the Catmull–Clark scheme, the limit surface only approximates a sphere. The considered control grid has extraordinary vertices of valence 3 and 5. We compute the mean curvature flow on the limit surface by solving the linear system described in Eq. (20) for a sequence of equidistant time steps. The evaluation is done using two isoparametric Catmull–Clark finite element approaches: the natural and the characteristic finite element approach. The first one is defined by the push-forward of the natural generating spline given in Definition 2.1. The natural shape functions b_j^N , $j = 0, \dots, K - 1$, on the surface patch Q are described by

$$b_j^N = b_j^* \circ s_Q^{-1},$$

where K is the number of vertices in the one-ring of the corresponding control grid element Q_c of Q . For the characteristic approach, the shape functions b_j^e are defined in Formula (10). In Fig. 9, we illustrate the resulting behaviour of the control grid

Table 1

Comparison of the assembly for the row-sum norm of the mass and stiffness matrices with 2^2 -, 3^2 - and 4^2 -point Gaussian quadrature for different subdivision levels using Theorem 3.1 (Level) and the Formula (12) (Rgl).

Lvl	Mass matrix			Stiffness matrix		
	2^2	3^2	4^2	2^2	3^2	4^2
3	1.367653	1.367680	1.367680	5.003495	5.015288	5.015259
5	1.387965	1.387993	1.387993	5.057578	5.069371	5.069342
7	1.389234	1.389262	1.389262	5.060777	5.072570	5.072541
9	1.389313	1.389341	1.389341	5.060977	5.072770	5.072740
11	1.389318	1.389346	1.389346	5.060989	5.072782	5.072753
Rgl	1.388859	1.389341	1.389350	4.797090	5.075389	5.072785

Table 2

Comparison of the assembly for the Frobenius norm of the mass and stiffness matrices with 2^2 -, 3^2 - and 4^2 -point Gaussian quadrature for different subdivision levels using Theorem 3.1 (Lvl) and the Formula (12) (Rgl).

Lvl	Mass matrix			Stiffness matrix		
	2^2	3^2	4^2	2^2	3^2	4^2
3	2.697433	2.697216	2.697221	9.120144	9.135855	9.135850
5	2.738202	2.737984	2.737989	9.230487	9.246130	9.246125
7	2.740755	2.740537	2.740542	9.237155	9.252794	9.252789
9	2.740914	2.740697	2.740702	9.237571	9.253209	9.253204
11	2.740924	2.740707	2.740712	9.237597	9.253235	9.253230
Rgl	2.750803	2.740237	2.740721	8.932965	9.253378	9.253310

Table 3

Comparison of the (max radius/min radius) ratio of the limit surface in time step t_1 , t_3 , t_5 and t_{10} of the mean curvature flow using characteristic and natural shape functions.

	t_1	t_3	t_5	t_{10}
Consistent	1.01050	1.00552	1.00314	1.00099
Natural	1.01791	1.01650	1.01228	1.00520

under the impact of the mean curvature flow using the two finite element approaches.

In addition, we examine the limit surface of the control grids emerging during the flow. Thinking of the flow effect, each point of the surface is moving in the mean curvature direction. This is, for a convex control grid, the limit surface becomes step-by-step more spherical. For the considered spherical control grids, the Catmull–Clark limit surface is an approximation of a sphere with an unknown radius. To get an impression of the deviation from this sphere, we calculate the (max radius/min radius) ratio. In Table 3, we show the ratios of the limit surface for a number of time steps. The evaluation of the limit surface has been done using ten by ten equidistant evaluation points over each element. For comparison, the ratio of the limit surface of the initial grid is 1.01568. In both cases, the limit geometry is more and more approaching a sphere. However, in the first step of the natural approach the ratio increases. In Fig. 10, the mean curvature of the initial limit surfaces and the limit surfaces for both shape function approaches at time t_{10} is shown. In order to obtain comparable curvature values, we scaled the initial grid to a sufficiently equal size. The colour coding illustrates the distribution of the mean curvature. It can be seen that with the characteristic approach the limit surface is more spherical than the two other surfaces.

In the last experiment, we consider a non-convex initial surface with genus two. The control grid has four extraordinary vertices with valence 6. By definition, any closed surface becomes spoiled in finite time. This means that the flow can only be continued smoothly for some finite time before singularities occur. We compute the mean curvature flow using the natural and characteristic finite elements. The impact of the flow for a number of steps is shown in Fig. 11. We compare the control grids and the limit surfaces of the two approaches. The surfaces are coloured by its mean curvature, this allow the investigation of the behaviour of limit surfaces in more detail. In both cases, the surface degenerates

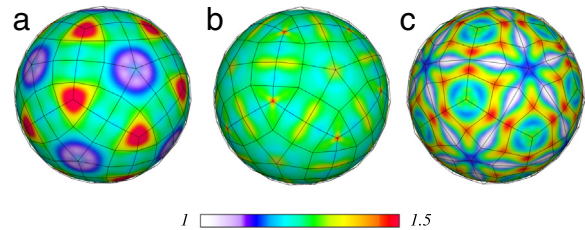


Fig. 10. Comparison of the mean curvature of the limit surface of (a) the initial grid (scaled by 0.8), (b) the grid at time t_{10} using characteristic shape functions and (c) the grid at time t_{10} using natural shape functions. The colours correspond to the values in the range [1, 1.5]. The distribution of the colour is shown by the colourbar. The evaluation of the surfaces is done via natural parameterization. (For interpretation of the references to colour in this figure legend, the reader is referred to the web version of this article.)

at the handles. However, using the natural elements the control grid differs from the initial grid and destroys more and more in the course of time. The distribution of the mean curvature on the handles indicates a perturbed surface behaviour. In contrast to this, the characteristic approach provides a non-destructive grid behaviour and a uniform shrinking of the surface. On the latter point, consider the manner in which the curvature distribute at the handles.

As the experiments show, the characteristic finite element approach is indicating a mesh behaviour conforming with the curvature flow. Comparing both approaches, there is a factor influencing the calculation. The factor is escorted by the pull-back domain of the finite elements. It emerges as the scaling factor λ of the partitioned domain (see Fig. 6) and influence the surface gradient defined in Theorem 3.2. For the natural finite element approach based on the natural generating spline, the factor is always the same and equals $\lambda = 1/4$, regardless of the valence of the extraordinary vertex. Whereas for the characteristic approach λ is changing depending on the extraordinary vertex valence. Keep in mind that λ is here the subdominant eigenvalue of the subdivision matrix. The matrix appears in the definition of the natural and characteristic generating spline, see Definitions 2.1 and 2.3, and is directly related to the finite element approach.

5. Conclusion and future work

The paper introduces a new subdivision finite element approach that is consistent with the classical idea of subdivision sur-

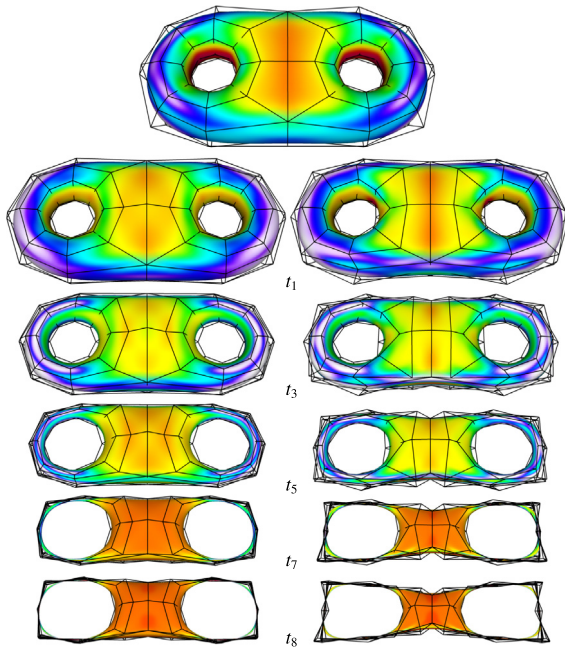


Fig. 11. Comparison of the impact of the characteristic and natural subdivision finite elements for the mean curvature flow on a non-convex surface with genus two. In the first row, the initial grid and its limit surface are shown. In the left and right column, the characteristic and the natural approaches, respectively, have been shown for a number of time steps t_i , $i = 1, 3, 5, 7, 8$. The range of the curvature corresponding to the colouring is changing with each step. Singularities appear at the handles, at time t_7 for the natural, and at time t_8 for the characteristic approach. (For interpretation of the references to colour in this figure legend, the reader is referred to the web version of this article.)

faces. The aim of this paper is to derive the mathematical principles of this approach to use it for PDEs on surfaces. In our approach, we make use of the labour-intensive characteristic parameterization of the limit surface. However, in the presented concepts the inversion of the characteristic map is done only implicitly, i.e. in the integral representation, it reduces to a valence dependent scaling factor. That makes our approach practicable for PDE applications. Due to the complexity of the to be integrated functions, the use of an appropriate numerical integration is still an open problem. On the other hand, the computational effort that accompanies the integration on irregular elements also indicates that more work needs to be done in this area. Moreover, a more valid explanation for the choice of the number of subdivision levels have to be found. In the future, we will investigate the dependence of the valence of the extraordinary vertex on the number of subdivision levels to be integrated.

One of the goals is to show our experience regarding the use of subdivision finite elements for PDEs on surfaces. The repeated application of finite elements indicates the behaviour of the approach close to singularities. Thus, the elaborated generating splines gives an insight into the integration requirements on irregular elements. In the experimental section, we concentrate on the mean curvature flow on closed surfaces. The results confirm the qualitative behaviour of our characteristic finite element

approach. An important application of the mean curvature flow is the construction of minimal surfaces. Hence, the flow is applied to surfaces with boundaries. A set of appropriate boundary constraints has to be considered. We consider this problem in a separate publication.

Acknowledgement

This research was supported by the DFG Collaborative Research Center SFB/TRR 109 “Discretization in Geometry and Dynamics” <http://www.discretization.de>.

References

- [1] Lane JM, Riesenfeld RF. A theoretical development for the computer generation and display of piecewise polynomial surfaces. *IEEE Trans Pattern Anal Mach Intell* 1980;2(1):35–46.
- [2] Reif U. A unified approach to subdivision algorithms near extraordinary vertices. *Comput Aided Geom Design* 1995;12(2):153–74.
- [3] Reif U, Schröder P. Curvature integrability of subdivision surfaces. *Adv Comput Math* 2001;14:157–74.
- [4] Peters J, Reif U. *Subdivision surfaces. Geometry and computing*, vol. 3. New York: Springer-Verlag; 2008.
- [5] Cashman TJ. Beyond Catmull–Clark? A survey of advances in subdivision surface methods. In: *Computer graphics forum*. Vol. 31. Wiley Online Library; 2012. p. 42–61.
- [6] Ma W. Subdivision surfaces for CAD—an overview. *Comput Aided Des* 2005;37:693–709.
- [7] Stam J. 1998. Evaluation of Loop subdivision surfaces. In: *SIGGRAPH'98 CD-ROM*.
- [8] Stam J. Exact evaluation of Catmull–Clark subdivision surfaces at arbitrary parameter values. In: *SIGGRAPH 98 conference proceedings, annual conference series*. New York, NY, USA: ACM; 1998. p. 395–404.
- [9] Cirak F, Ortiz M, Schröder P. Subdivision surfaces: a new paradigm for thin-shell finite-element analysis. *Internat J Numer Methods Engrg* 2000;47(12):2039–72.
- [10] Barendrecht PJ. *Isogeometric analysis with subdivision surfaces*. Eindhoven: Eindhoven University of Technology; 2013.
- [11] Nguyen T, Karčiauskas K, Peters J. A comparative study of several classical, discrete differential and isogeometric methods for solving Poisson's equation on the disk. *Axioms* 2014;3(2):280–99.
- [12] Catmull E, Clark J. Recursively generated B-spline surfaces on arbitrary topological meshes. *Comput Aided Geom Design* 1978;10:350–5.
- [13] Boier-Martin I, Zorin D. Differentiable parameterization of Catmull–Clark subdivision surfaces. In: *Proceedings of the 2004 Eurographics/ACM SIGGRAPH symposium on geometry processing*. ACM; 2004. p. 155–64.
- [14] Cirak F, Ortiz M. Fully C1-conforming subdivision elements for finite deformation thin-shell analysis. *Internat J Numer Methods Engrg* 2001;51(7):813–33.
- [15] Cirak F, Scott MJ, Antonsson EK, Ortiz M, Schröder P. Integrated modeling, finite-element analysis, and engineering design for thin-shell structures using subdivision. *Comput-Aided Des* 2002;34(2):137–48.
- [16] Burkhart D, Hamann B, Umlauf G. Iso-geometric finite element analysis based on Catmull–Clark subdivision solids. *Comput Graph Forum* 2010;29(5):1575–84.
- [17] Wawrzinek A, Hildebrandt K, Polthier K. Koiter's thin shells on Catmull–Clark limit surfaces. In: *VMV 2011: Vision, modeling & visualization*. Berlin, Germany: Eurographics Association; 2011. p. 113–20.
- [18] Wei X, Zhang Y, Hughes TJ, Scott MA. Truncated hierarchical Catmull–Clark subdivision with local refinement. *Comput Methods Appl Mech Engrg* 2015;291:1–20.
- [19] Jüttler B, Mantzaflaris A, Perl R, Rumpf M. On numerical integration in isogeometric subdivision methods for PDEs on surfaces. *Comput Methods Appl Mech Engrg* 2016.
- [20] Riffnaller-Schiefer A, Augsdörfer U, Fellner D. Isogeometric shell analysis with NURBS compatible subdivision surfaces. *Appl Math Comput* 2015.
- [21] Peters J, Reif U. Analysis of algorithms generalizing B-spline subdivision. *SIAM J Numer Anal* 1998;35(2):728–48.
- [22] Zorin DN. *Stationary subdivision and multiresolution surface representations* (Ph.D. thesis), California Institute of Technology; 1998.
- [23] Strang G, Fix GJ. *An analysis of the finite element method*, Vol. 212. Englewood Cliffs, NJ: Prentice-Hall; 1973.